

Plasma-deposited AgOx-doped TiOx coatings enable rapid antibacterial activity based on ROS generation

Dirk Hegemann¹  | Barbara Hanselmann¹ | Flavia Zuber²  | Fei Pan²  |
Sandra Gaiser¹  | Patrick Rupper¹  | Katharina Maniura-Weber²  |
Kurt Ruffieux³ | Qun Ren² 

¹Laboratory for Advanced Fibers, Empa, Swiss Federal Laboratories for Materials Science and Technology, St. Gallen, Switzerland

²Laboratory for Biointerfaces, Empa, Swiss Federal Laboratories for Materials Science and Technology, St. Gallen, Switzerland

³MedTecton GmbH, Luzern, Switzerland

Correspondence

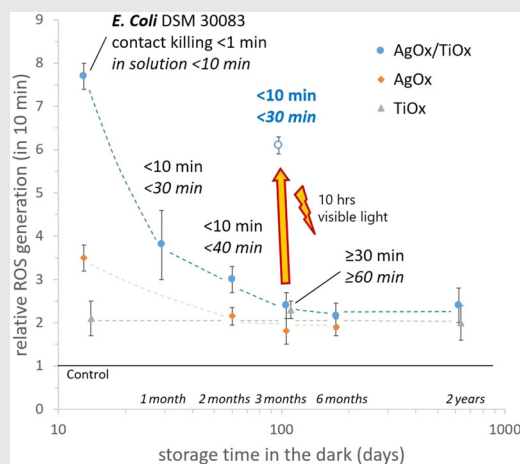
Dirk Hegemann, Plasma & Coating Group, Empa, 9014 St. Gallen, Switzerland.
Email: dirk.hegemann@empa.ch

Funding information

Innosuisse – Swiss Innovation Agency, Grant/Award Number: Project no. 30078.1 IP-LS

Abstract

To enable a rapid-acting antibacterial mechanism without the release of biocidal substances, TiO₂ catalysts have been considered based on the generation of reactive oxygen species (ROS). Doping with dissimilar metals generates electron-hole pairs with narrow band gaps promoting the production of ROS. Here, plasma technology is investigated to deposit Ag nano islets on defective TiOx films, stabilized by plasma postoxidation suppressing Ag ion release. Importantly, ROS generation is maintained upon storage in the dark yet with diminishing efficacy; however, it can be restored by exposure to visible light. The rapid-acting antibacterial properties are found to strongly correlate with ROS generation, which can even be maintained by functionalization with hydrophobic plasma polymer films. The cytocompatible coatings offer promising applications for implants and other medical devices.



KEYWORDS

antibacterial efficacy, biocompatibility, catalytic activity, metal oxides, ROS generation

This is an open access article under the terms of the Creative Commons Attribution-NonCommercial License, which permits use, distribution and reproduction in any medium, provided the original work is properly cited and is not used for commercial purposes.

© 2022 The Authors. *Plasma Processes and Polymers* published by Wiley-VCH GmbH.

1 | INTRODUCTION

Healthcare acquired infections (HAI) are a major burden for patients and healthcare costs. A large part of HAI is associated with percutaneous medical devices, such as venous and urinary catheters, as well as respiratory support devices, but many other external interfaces in the clinical setting have to be considered as well.^[1,2] To reduce HAI, critical devices are equipped with antibacterial properties, such as adding silver to kill bacteria through the released Ag^+ ions.^[3] To allow for biocompatible surfaces, that is, to maintain a silver release below potential toxicity levels, tight control over the amount of silver, its distribution, and chemical state is required, which can be achieved by various plasma-based methods.^[4–6] Yet, concerns exist about the use of antibacterial releasing systems also related to different and changing regulations, thus demanding for minimally or nonleaching systems.^[7] Metal oxide surfaces generating reactive oxygen species (ROS) might provide such antibacterial systems. For example, the use of TiO_2 and/or ZnO-born photocatalytic processes for their antibacterial properties have been explored.^[8,9] Photoexcitation of the semiconductor catalyst promotes electron (e^-) transfers from the valence band (VB) to the conduction band (CB), leaving behind a positive hole (h^+), thus creating a specific electron-hole pair that exhibits redox properties.^[10,11] At the catalytic surface, strong oxidizing radicals can be generated when H_2O and O_2 are present. Electron transfer to (dissolved) O_2 creates the superoxide anion, $^{\bullet}\text{O}_2^-$, by oxygen reduction reactions at the CB, while H_2O is oxidized by holes at the VB to form hydroxyl radicals, $^{\bullet}\text{OH}$. These short-living radicals induce further ROS, such as singlet molecular oxygen, $^1\text{O}_2$, and hydrogen peroxide, H_2O_2 , by electron transfer or recombination.^[12] Such species efficiently oxidize proteins and lipids in an aqueous environment, thus inactivating bacteria, as well as fungi and viruses.^[7,13–15]

The presence of oxygen vacancies in the metal oxide materials as in defective TiO_2 (also denoted as TiO_{2-x}) supports the separation of photoexcited charges since the energy band gap becomes narrowed, thus promoting the photocatalytic performance to generate ROS.^[16] Mostly, stabilized O vacancies, which are compensated by the presence of Ti^{3+} centers, can be obtained by doping with another semiconductor material generating electron-hole pairs with narrow band gaps.^[17,18] The cocatalyst hinders filling of oxygen vacancies and hydroxyl termination as occurring on TiO_2 due to the high reactivity of the intermediates, $^{\bullet}\text{O}_2^-$ and $^{\bullet}\text{OH}$, and combined $\text{O}_2/\text{H}_2\text{O}$ reactions.^[19]

Importantly, plasma processing promotes the formation of Ti^{3+} and O vacancies in nonstoichiometric TiO_x related to the ion bombardment during film growth when deposited at low temperatures.^[20–22] Furthermore, plasma posttreatment was found to induce oxygen vacancies in TiO_2 either by using a reducing gas (H_2 plasma) or an oxidizing gas (air plasma).^[23,24] Most of all, the use of plasma processing to deposit TiO_2 (or TiO_x) as support doped by another semiconductor material, such as Cu, Fe, Co, or Ag oxides, enables the stabilization of the catalytic metal oxide compound by retarding charge recombination.^[15,24–26] As a consequence, not only O vacancies are stabilized but also the possible release of metal ions is suppressed, promoting ROS generation at low light conditions and even in the dark, likely due to electron transfer from Ti^{3+} sites to adsorbed molecules and synergetic interaction of the O vacancies with the doped oxidized metal.^[27] Furthermore, it has long been recognized that the high surface-to-volume ratio of nanostructures leads to a decrease in the hole-electron recombination rate as in TiO_2 and a faster interfacial charge carrier transfer rate.^[28] Yet only recently, the understanding of enhanced electron transfer processes at edges and corners of heterogeneous nanostructures contributing to oxygen reduction reactions has been improved.^[29]

In this study, plasma technology is investigated to deposit Ag nano islets on TiO_x films by magnetron sputtering followed by plasma postoxidation to directly generate O vacancies and Ag_2O nanostructures having a large interface area with the support. As substrates, typical materials for catheters such as polyurethane and silicone were considered. It was observed that the generation of ROS strongly correlates with the antibacterial efficacy of the metal oxide surfaces with negligible leaching of metal ions, resulting in rapid killing of bacteria in contact and in solution. The ability to produce ROS was followed over two years during storage in the dark. While low activity was still maintained, the rapid-acting antibacterial mechanism could be restored by visible light exposure.

Finally, the potential to tune surface wettability by plasma polymer deposition on the metal oxide surface is investigated as a novel approach, as it is well known that wettability influences the adhesion of bacteria to abiotic surfaces, often showing reduced adhesion on silicone-based hydrophobic surfaces following the so-called Baier curve.^[30] A 4-nm-thin hydrophobic plasma polymer layer using hexamethyldisiloxane (HMDSO) as the monomer was deposited on the ROS generating metal oxide surface, and the antibacterial effect was found to still maintain. Such novel multifunctional surfaces open a wide range of potential applications.

2 | EXPERIMENTAL SECTION

2.1 | Plasma processing

A low-pressure pilot-scale reactor was used for plasma deposition of TiOx and AgOx films, allowing plasma cleaning/activation, magnetron sputtering from Ti and Ag targets, and plasma postoxidation, which can be subsequently performed in a one-step process.^[31] Here, the notation TiOx and AgOx is used to indicate a rather unspecified oxidized Ti or Ag state, which might comprise different or varying oxidation degrees, for example, with depth, location, and aging.

Briefly, the used reactor contained a rotatable drum (70 cm width, 60 cm in diameter) as RF-driven (13.56 MHz) electrode and two places for targets (8 cm distance to the drum electrode) with a water-cooled magnetron sputtering device. The samples were attached to the drum electrode, and the chamber was evacuated to 10^{-3} Pa. After cleaning with Ar plasma (10 min, gas flow rate of 160 sccm, RF power of 400 W, 10 Pa), an about 25-nm-thick layer of TiOx was sputtered from a metal target ($76 \times 15.5 \text{ cm}^2$) by Ar plasma (70 sccm, no O₂ added) using a rotation speed of 0.3 m/min in front of the first Ti target (pulsed DC magnetron, 2000 W, 320 V, 0.8 Pa). Residual oxygen and water (as well as oxidation at ambient air) result in the formation of nonstoichiometric TiOx.^[20] Such TiOx coatings were taken as reference, while for the Ag/TiOx coatings, an additional on average 4-nm-thick Ag layer ($4 \mu\text{g cm}^{-2}$) was subsequently sputtered from a silver target by Ar plasma (70 sccm) using a rotation speed of 3 m/min in front of the second target (DC magnetron, 600 W, 400 V, 0.8 Pa). The deposited Ag formed distinct nano islets consisting of metal silver (Ag⁰).^[32] To oxidize the Ag/TiOx coating, plasma postoxidation was applied in an Ar/O₂ plasma (10 min, 160/40 sccm, 500 W, 10 Pa), yielding AgOx-doped TiOx coatings. Metallic and oxidized Ag nano islets with 4 nm average thickness were also used as reference deposited without the underlying TiOx film.

The 4-nm hydrophobic cover layer was deposited by plasma-enhanced chemical vapor deposition following an established protocol (10 s, Ar/HMDSO 20/4 sccm, 50 W, 7 Pa).^[33–35] All plasma process steps were performed at low temperature (<70°C), thus allowing treatment of sensitive materials, such as polymers, textiles, nonwovens, or scaffolds.

Various substrate materials have been selected, such as Si wafers and glass slides for characterization and medical-grade thermoplastic polyurethane (TPU) and silicone materials as used for urethral devices and catheters. All coatings showed excellent adhesion following an appropriate cleaning method. The metal oxide coatings can also

be deposited on other fibrous materials (including nonwovens and nanofibrous membranes), largely maintaining their mechanical properties.^[32,36] After the plasma processing, the samples were stored in polypropylene bags in a dark, ambient environment for different periods up to 2 years. For characterization, samples were cut and provided within minutes to avoid extended exposure to light and possible catalyst reactivation unless light exposure was examined on purpose.^[37]

2.2 | Surface characterization

The morphology of the samples was investigated by scanning electron microscopy (SEM) using a Hitachi S-4800 microscope operating at accelerating voltages of 2 kV. The weakly conductive samples were imaged without applying an additional conductive layer.

X-ray photoelectron spectrometry (XPS) measurements were performed with a Scanning XPS Microprobe (PHI VersaProbe II spectrometer, Physical Electronics) with monochromatic Al K α radiation (1486.6 eV) in combination with argon ion depth profile sputtering.^[20,36] A photoemission take-off angle of 45° (with respect to the sample surface) was used. Operating pressure was below 5×10^{-7} Pa. The samples directly adhered to a stainless steel holder via a double-sided tape and a randomly chosen spot for each sample was analyzed using a micro-focused X-ray beam of diameter 100 μm (25 W at 15 kV). Sample charging was compensated using dual beam charge neutralization and the obtained spectra were shifted relative to the aliphatic carbon (C–C) at 285.0 eV. Survey scan spectra (0–1100 eV) were acquired with an energy step of 0.8 eV, an acquisition time of 160 ms/data point, and an analyzer pass energy of 187.85 eV. Higher-resolution regional spectra were acquired of C 1s, O 1s, Ti 2p, and Ag 3d using an energy step of 0.125 eV, an acquisition time of 1.9 s per data point, and an analyzer pass energy of 29.35 eV. Under these conditions, the energy resolution (FWHM, full width at half-maximum height) measured on the Ag 3d^{5/2} line is 2.2 eV (surveys) and 0.7 eV (regions), respectively. Intensity determination and curve fitting was carried out with CasaXPS (software version 2.3.16) using a fixed 70% Gaussian, 30% Lorentzian product function, and a Shirley-type background to fit the XPS spectra. More details about the XPS system and measurement conditions have been previously published.^[38] Here, the Ti 2p spectrum was fitted using eight components, four each belonging to the 2p_{3/2} and 2p_{1/2} spin-orbit components, and representing different Ti oxidation states: Ti(4) (TiO₂), Ti(3) (Ti₂O₃), Ti(2) (TiO), and Ti(0) (metallic). The energetic positions of the four bands for 2p_{3/2} were fixed to literature values (454.1 eV for Ti(0),

455.3 eV for Ti(2), 457.2 eV for Ti(3) and 459.2 eV for Ti(4).^[39] The four bands for $2p_{1/2}$ had a fixed energy separation to the corresponding bands of $2p_{3/2}$, where the shift was taken from the literature value as 5.54 eV (for Ti oxides) and 6.17 eV (for Ti metal).^[40] The intensity ratio between the $2p_{3/2}$ and the $2p_{1/2}$ component was fixed to the theoretical value of 2:1.

The silver release was assessed by storing samples of 10 cm^2 in 4 ml ultrapure water for different periods at room temperature in the dark. The resulting eluate was analyzed by Inductively Coupled Plasma—Optical Emission Spectroscopy (ICP-OES) using an Optima 3000 device from Perkin Elmer (Ag lines at 328.068 and 338.289 nm). The calibration was performed using an external silver standard solution of 1 g L^{-1} . Static water contact angles were measured by depositing water drops ($2\text{ }\mu\text{l}$) using a Krüss, DSA25 device averaging over a minimum of three measurements at different places on the sample surface.

2.3 | Determination of ROS

To detect ROS generated from the coated samples, the fluorogenic dye dihydrorhodamine 123 (DHR 123) was used as it indicates the detection of peroxides (and peroxy-nitrites) by producing the fluorescent rhodamine 123, while it does not react with superoxide radicals.^[41] For comparison, dihydroethidium (DHE) was also considered, a fluorogenic dye useful for detecting any ROS, such as species of superoxide-, peroxide-, and peroxy-nitrite-mediated oxidative chemistry.^[41] The measurement was carried out according to the dye manufacturer's instructions. Briefly, three replicates of each sample and controls were placed in a 48-well plate and immersed in 0.9 ml deionized water.^[42] 0.1 ml DHR 123 is added to the wells ($100\text{ }\mu\text{M}$, to achieve the final $10\text{ }\mu\text{M}$). The fluorescence reading at zero time point was immediately taken (DHR: excitation at 488 nm, emission at 535 nm; DHE: 358/461 nm). Subsequently, the fluorescence readings of all samples were obtained after 10 min, and the fluorescence ratio was calculated compared to the initial control (TPU reference). Thereby, three technical repeats of $50\text{ }\mu\text{l}$ each were pipetted and quantified with the fluorescent spectrometer for each replicate. Selected samples were also measured after 20 and 30 min showing a steady (nonlinear) increase of ROS generation.

2.4 | Assessment of antibacterial properties

Antibacterial activity was first qualitatively assessed by agar diffusion assay for the leaching effects and touch

test for contact killing.^[43] Samples were punched into 9 mm disks aseptically and immediately used for antimicrobial testing. The Gram-positive bacteria *Staphylococcus aureus* MRSA and the Gram-negative *Escherichia coli* DSM 30083 were used here as two representative pathogens.^[44,45] Bacteria colonies from an agar plate were incubated in Tryptic Soy Broth + 0.25% Glucose (TSB) at 37°C overnight. The overnight culture was diluted to an $\text{OD}_{600\text{ nm}}$ of 0.1 in 5 ml fresh TSB and cultivated for around 2 h until an exponential growth phase was reached. The bacterial cultures were diluted with sterile 0.9% NaCl to around 10^6 colony forming units (CFU) ml^{-1} . Hundred microliters of bacterial suspension were spread on a PC-agar plate, and triplicates of samples to be tested were placed on the agar after the bacterial lawn was allowed to dry. The agar plates with samples were then incubated at 37°C overnight. Right after, the growth inhibition zone was analyzed. In parallel, for the touch test to evaluate the ability for contact killing, the samples were placed on top of agar in triplicates for a defined time (1, 10, and 30 min) and then removed. The bacterial growth on the touched area was analyzed after overnight incubation at 37°C .

The antibacterial efficacy was further measured quantitatively following a modified ASTM (American Society for Testing and Materials) method as reported previously.^[46] Hundred microliters of bacterial suspension in 0.9% NaCl with about 10^6 CFU ml^{-1} was loaded on the surface of the sample of 9 mm diameter (0.64 cm^2) and incubated at 37°C for 10–60 min. The suspension was subsequently removed, and the samples were washed twice with 1 ml phosphate-buffered saline (PBS) to remove the adhered bacteria. The removed bacterial suspension and the washing solution from each sample were collected and mixed. The washed samples were placed in 2.5 ml 1x PBS, sonicated for 5 min, and thereafter vigorously vortexed for 15 s. Serial dilutions of the two collected bacterial mixtures were spotted on PC agar plates. All plates were incubated at 37°C overnight. Bacterial colonies were counted subsequently after overnight incubation to obtain an estimation of the viable cells on each of the samples. Again, for each measurement, three samples were analyzed to obtain an average value.

2.5 | Cytotoxicity assay

Cytotoxicity of the plasma-coated samples was analyzed using normal human dermal fibroblasts (NHDFs; C-12352; PromoCell) following the ISO10993-5 norm. Samples were extracted in DMEM (Dulbecco's Modified Eagle Medium) containing 1% penicillin/streptomycin/neomycin with an extraction ratio of the surface area per

medium volume of $3 \text{ cm}^2 \text{ ml}^{-1}$. Empty wells without any sample were used as the negative control. The extraction process was carried out at 37°C with 100% humidity and 5% CO_2 for 1, 10, and 60 min. NHDFs were seeded with 10 000 cells per well (TPP) in $100 \mu\text{l}$ DMEM containing 10% fetal calf serum (FCS) 1 day before incubation with extracts. The NHDFs were then incubated for 24 h with $100 \mu\text{l}$ (95% extract + 5% FCS) by replacing the old media. The viable NHDFs cells of negative control were set as 100%, and the ones incubated with 1% Triton X-100 in DMEM containing 5% FCS were regarded as the positive control. Cell viability was measured using MTS [(3-(4,5-dimethylthiazol-2-yl)-5-(3-carboxymethoxyphenyl)-2-(4-sulfophenyl)-2H-tetrazolium)] assay via the absorbance at 490 nm.

3 | RESULTS AND DISCUSSION

3.1 | Plasma deposition of metal oxide catalysts

Using magnetron sputtering from metal targets and optionally plasma post-oxidation, four different samples were produced and further investigated: (i) 4-nm-thick (on average) metallic silver (Ag^0), (ii) plasma-oxidized 4 nm silver coating (AgOx), (iii) ~ 25 -nm-thick TiOx film, oxidized at ambient air and used as a reference, and (iv) 4 nm of Ag deposited on ~ 25 nm TiOx and plasma-oxidized (AgOx/TiOx). At first, the morphology of the samples was analyzed by SEM 1 day after deposition, as presented in Figure 1. Ag^0 formed nonclosed silver islands on the different substrates that changed their appearance after plasma oxidation, forming more

pronounced nano islands. At the same time, the metallic appearance as seen by the plasmonic brownish color vanished. When deposited on TiOx as support, the Ag dopant formed particular nanostructures, named Ag nano islets, upon plasma oxidation. TiOx itself revealed a smooth surface.

The chemical binding state of the different samples was analyzed by XPS, as displayed in Figure 2. For Ag^0 , the binding energies were detected at 368.8 eV ($\text{Ag } 3d_{5/2}$) and 374.7 eV ($\text{Ag } 3d_{3/2}$), thus slightly higher than generally reported for metallic silver.^[47] This might be caused by the nano character of the deposit as a positive shift in binding energies has been reported for Ag nanoparticles of size 20–100 nm.^[48] Plasma oxidation yielded a negative shift of ~ 0.5 eV, indicating the formation of a silver oxide (Figure 2a), which might mainly be Ag_2O but likely not pure.^[47,49]

The TiOx coating was sputtered from a metallic Ti target in an Ar plasma (without O_2 addition). However, a highly nonstoichiometric TiOx was formed as indicated by the spin-orbit components that are not clearly resolved due to the partial overlap between highly oxidized components of $\text{Ti } 2p_{3/2}$ with lower oxidized components of $\text{Ti } 2p_{1/2}$ (Figure 2b). Due to the partial overlapping of the individual Ti oxidation states and the possible presence of intermediate species after short sputtering of the TiOx surface in the XPS device, FWHM of the different Ti components varied mainly between 1.5 and 2.3 eV, with the Ti metal peak having a slightly narrower bandwidth than the oxides. Oxidation processes during deposition (by residual oxygen in the reactor) and mainly after deposition (by exposure to ambient air) account for TiO_2 formation at the outermost surface with increasing metallic character in depth.^[20] Note that this gradient in

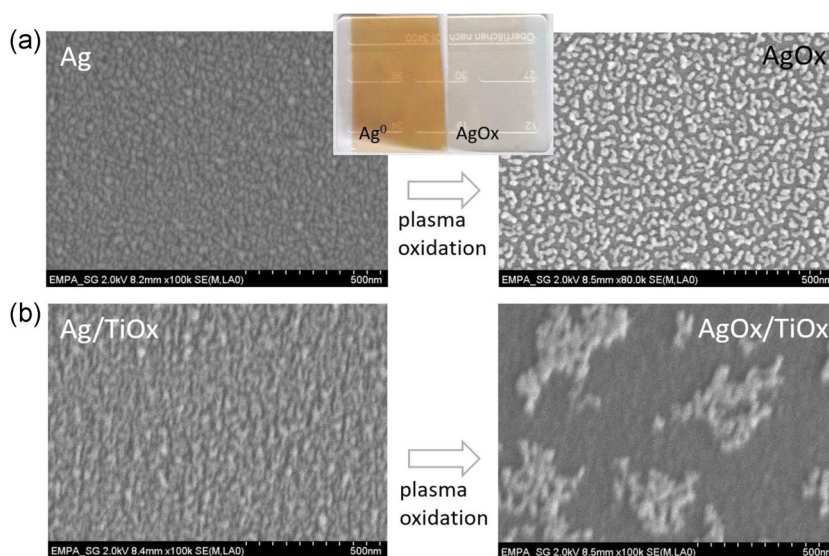


FIGURE 1 Scanning electron microscopy images of sputter-deposited coatings on Si wafer. (a) a 4-nm-thick Ag film as-deposited and after plasma post-oxidation, yielding the formation of pronounced nano islands. The inset picture displays the plasmonic color of the metal Ag film that vanishes upon oxidation. (b) The same Ag film as-deposited on the TiOx support. Plasma postoxidation results in the formation of nano islets offering a large interface area

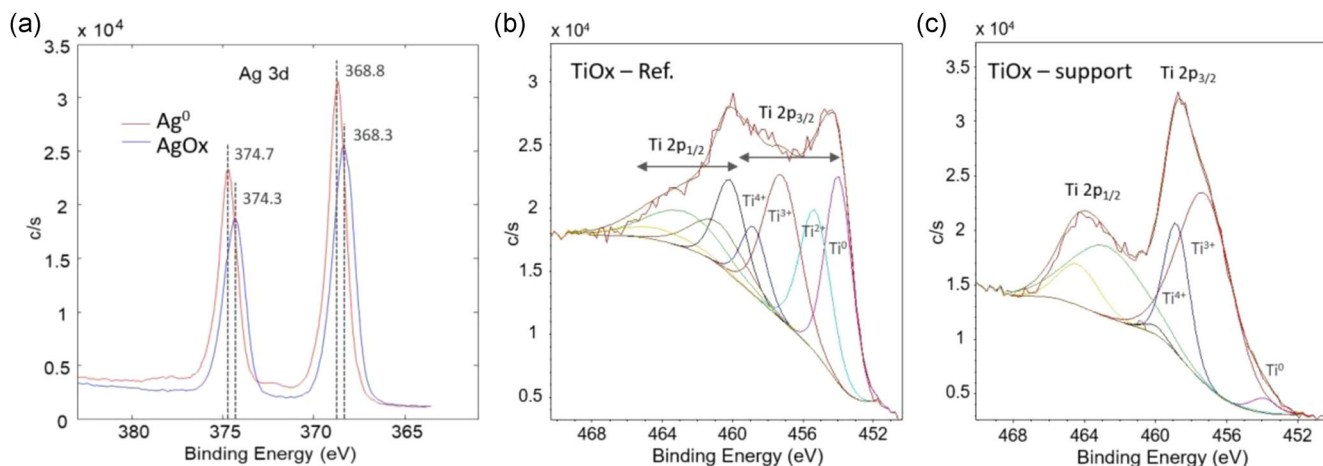


FIGURE 2 X-ray photoelectron spectroscopy spectra: (a) Four nanometers of Ag⁰ as-deposited and plasma-oxidized (AgOx) resulting in a shift of the binding energies, (b) nonstoichiometric TiO as-deposited for reference (without plasma oxidation), and (c) plasma-oxidized TiOx used as support for AgOx/TiOx. Note that short Ar sputtering (2 kV beam voltage) was used for spectra (b) and (c) before the measurement

chemical composition effectively hinders photocatalytic degradation of underlying polymeric substrates. To examine the effect of plasma post-oxidation as applied after Ag deposition, the oxidized TiOx samples were again shortly sputtered within the XPS device to detect the near-surface composition. As seen in Figure 2c, plasma oxidation produced a distinct defective TiOx film (also named TiO_{2-x}) characterized by a high amount of Ti³⁺ (accompanied by O vacancies) besides Ti⁴⁺ (TiO₂) with a lower metallic character than the nonoxidized reference.^[21,22,50] The selected amount of Ag as dopant on the TiOx support thus provides a promising catalyst with a large interface area between the oxidized Ag nano islets and the defective TiOx.

3.2 | ROS generation

The metal oxide samples were tested for their ability to produce ROS, as depicted in Figure 3. Since H₂O₂ can be expected to be the most stable ROS produced from the highly reactive intermediates, [•]O₂⁻ and [•]OH,^[51] mainly the fluorogenic dye DHR 123 was used to detect the relative ROS generation in water. In addition, TiOx nanostructures were reported to noticeably produce H₂O₂ as an antimicrobial agent.^[52,53] For samples stored for 2 weeks in the dark, DHE covering ROS in general, was used as well. As a non-ROS-producing reference, a TPU sample was taken, and the obtained signal was arbitrarily set to one. The comparison of DHR and DHE for plasma-oxidized Ag and AgOx-doped TiOx demonstrated—as expected—higher ROS signals using DHE, which even became more pronounced by measuring after 30 min.

The catalyst AgOx/TiOx clearly outperformed AgOx (Figure 3a). Relative ROS measurements for different samples after different storage periods in the dark were collected using DHR (Figure 3b). The catalytically active coating AgOx/TiOx initially produced high amounts of ROS that were slowly attenuated upon storage in the dark followed over 2 years. Oxidized Ag coatings also revealed enhanced ROS generation in the beginning, while the less reactive, nonstoichiometric TiOx reference showed a low yet continuous ROS generation (higher than the TPU reference), probably owing to its metastable state, as also known from TiOx nanoparticles.^[52] Likewise, Ag₂O is known to be chemically reduced during its catalytic activity but becomes stabilized when a certain amount of Ag⁰ is formed, promoting continuous mild ROS generation.^[54]

Most of all, the AgOx-doped TiOx samples offer narrow band gaps supported by oxygen vacancy states, as schematically shown in Figure 4.^[16,55] Hence, [•]O₂⁻ and [•]OH radicals should be readily produced by electron transfer at the CB of TiOx and AgOx and oxidation by holes at the VB, mainly on heterogeneous nanostructures. Such radicals further react to singlet molecular oxygen and hydrogen peroxide. The ROS measurements indicate that the ability for such reactions might well be preserved even during storage in the dark, whereby extended interaction times in water still produced significant amounts of ROS, as demonstrated after about 100 days of storage. Similar reactions can be expected for the plasma-oxidized Ag nanocoating and the TiOx reference. Importantly, the samples can restore their ROS generation capability after exposure to visible light (indoor lighting), even after extended storage times in the dark.

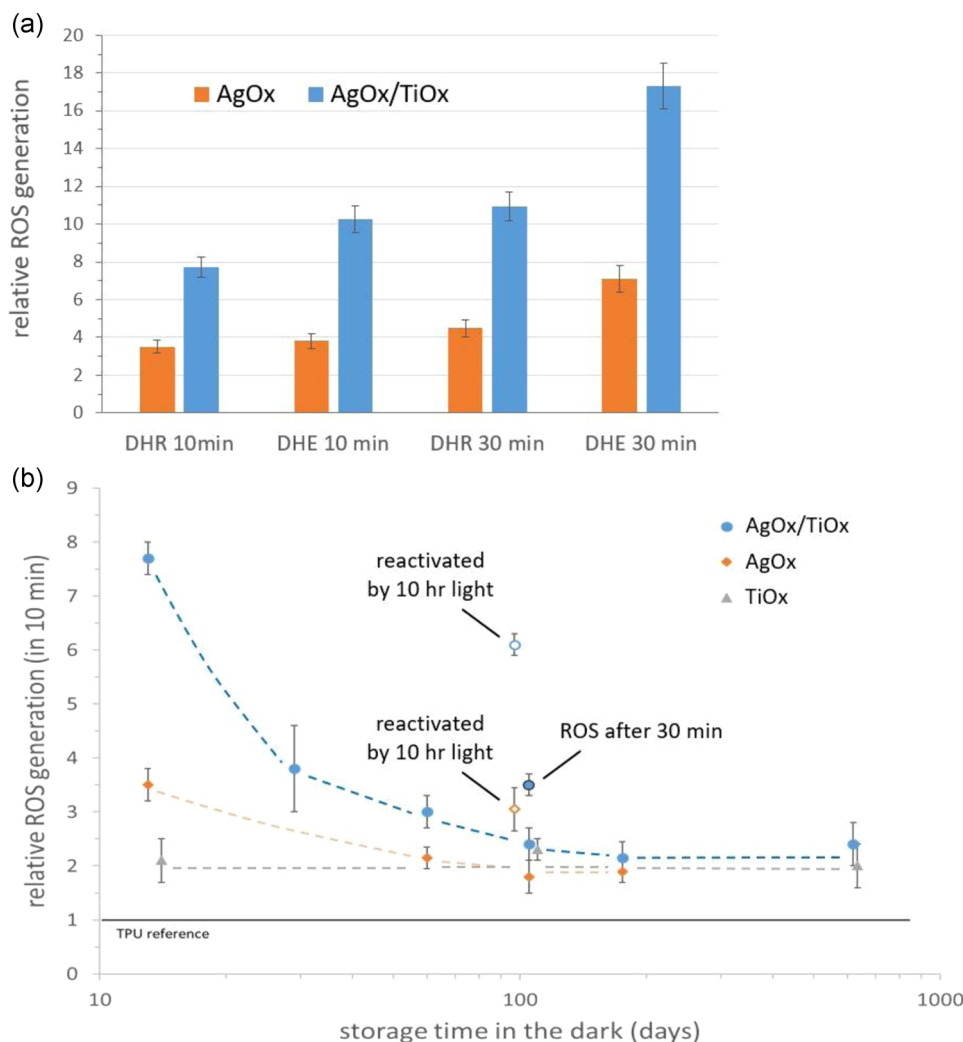


FIGURE 3 ROS generation as measured by fluorogenic dyes in water relative to a TPU control (arbitrarily set to 1). (a) Comparison of the two dyes: DHR (more specific for H_2O_2) and DHE (index for overall ROS generation), measured after 10 and 30 min. Samples were stored for 2 weeks in the dark. (b) DHR after 10 min, versus storage time in the dark. The dark-lined dot shows one ROS measurement after 30 min. One AgOx/TiOx and one AgOx sample were reactivated by exposure to visible light (indoor lighting), yielding enhanced ROS generation again. DHE, dihydroethidium; DHR, dihydrorhodamine; ROS, reactive oxygen species; TPU, thermoplastic polyurethane

3.3 | Antibacterial efficacy

The antibacterial activity of the metal oxide coatings was assessed qualitatively using an agar diffusion assay and an agar touch test to study the activity caused by active agents leached from coatings and/or by contact killing at the coating surface (Figure 5). Samples stored for different periods at ambient conditions in the dark were studied. All tested samples after storage for 2 weeks, including TPU and Ag^0 , did not lead to any visible inhibition zone of *E. coli* and *S. aureus* in the agar diffusion assay around the spots where the three samples had been placed, suggesting that the plasma-coated samples did not release antibacterial agents during overnight incubation.

To investigate the possible rapid contact killing mechanism, a contact time of 10 min between samples

and bacteria was selected first for the touch test to qualitatively assess the degree of overgrowth after removal of the triplicate samples. No visible inhibition of bacterial growth was noticed within this short time for the control sample TPU and Ag^0 , while reduced growth of *E. coli* but not of *S. aureus* was found for the TiOx reference. On the contrary, the oxidized Ag film and, most of all, the AgOx-doped TiOx demonstrated a high antibacterial activity already within 10 min of contact, revealing a stronger effect against both *E. coli* and *S. aureus*.

Different storage periods and different contact times were then investigated for AgOx/TiOx coatings interacting with *E. coli* (Figure 6). Freshly deposited coatings demonstrated a rapid action against *E. coli* by completely killing within 1 min as observed by the three dark spots in the touch test where the samples had been placed.

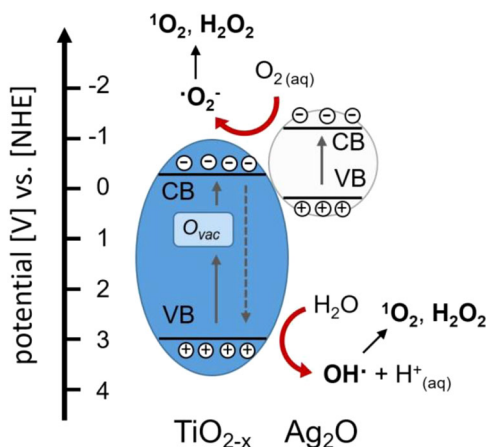


FIGURE 4 Schematic representation of the interfacial charge transfer to adsorbed O_2 and H_2O of Ag_2O supported on TiO_2 , yielding reactive oxygen species generation. Oxygen vacancies in TiO_2 and doping by oxidized Ag allow narrow band gaps and thus activation in low-light conditions. CB, conduction band; VB, valence band

However, a small inhibition zone was detected in the diffusion assay, indicating a low release of Ag ions during overnight incubation. For samples stored for 2 weeks in the dark, this releasing effect fully disappeared, while the same coatings still revealed rapid action after 1 min and excellent inhibition after 10 min (see Figure 5a). The antibacterial efficacy was then maintained during at least 2 months of storage in the dark.

The AgOx/TiOx coating showed a similar behavior when tested against *S. aureus* (data not shown); however, with stronger antibacterial activity against *E. coli*. This difference is likely caused by the different membrane structure of the Gram-negative (*E. coli*) and -positive (*S. aureus*) bacterial species, which has been reported to respond to ROS with different inactivation kinetics.^[46] Furthermore, *S. aureus* uses several defensive molecules to counteract ROS.^[9] Samples stored for 100 days in the dark showed full bacterial overgrowth with a contact time of 10 min, yet they revealed a minor inhibition for both strains when the contact of the samples with bacteria was extended to 30 min (data not shown). Importantly, the AgOx/TiOx catalytic surfaces could be reactivated by visible light. Exposure to indoor lighting for 10 h restored the contact killing activity of the samples stored for 100 days and repeated after storage for 8 months in dark conditions (Figure 6).

Quantitative analysis of the antibacterial efficacy of the metal oxide coatings was further performed using a bacterial suspension as described in Section 2. The short-time stored AgOx/TiOx samples (2 weeks in the dark) clearly showed a rapid antibacterial activity, which led to more than 1 and 4 log reduction of viable cells after

10 and 30 min interaction, respectively. After 60 min, the viable cells were completely eliminated and impossible to measure anymore (Figure 7a). Samples produced in different runs demonstrate the good repeatability of the coating procedure. The samples stored for 1 month still allowed rapid-acting bacterial inhibition with about 2 log and more than 4 log reduction of the viable cells after 30 and 60 min, respectively (Figure 7b). With longer storage times in the dark, the antibacterial effect required increasing interaction times. Even after 100 days of storage the samples still exhibited a minor activity within 1 h (Figure 7c). Similar antibacterial activity was observed when NaCl was added or urine was used as a solution (data not shown).

From the comparison of the antibacterial efficacy with the attenuation of the ROS signal during storage in the dark, it can be inferred that the rapid-acting antibacterial mechanism as observed for the examined metal oxide coatings is based on ROS generation. This finding is further supported by the absence of an inhibition zone in the diffusion assay. The observation of a minor inhibition zone as noted for the highly reactive, metastable AgOx/TiOx coatings tested shortly after deposition might indicate that a small amount of chemisorbed Ag ions was present at the surface that initially can be released, while it gets stabilized within a few days.^[56] SEM images corroborate this assumption as demonstrated in Figure 8, revealing that the smallest Ag islands observed on freshly prepared AgOx/TiOx samples quickly disappeared during storage. Hence, it can be expected that Ag ion release did not contribute to the observed rapid-acting antibacterial efficacy, whereas ROS generated at the biointerface yields contact killing and diffusion of ROS is responsible for bacterial inhibition in solution.

3.4 | Silver release and biocompatibility

To further demonstrate the minimally leaching properties of the metal oxide catalyst, the Ag ion release was determined by ICP-OES after different periods of incubation in ultrapure water. To this end, the investigated AgOx -doped TiOx coating was compared to an Ag^0 coating (without TiOx support) that was previously optimized for a controlled Ag ion release (Figure 9). The latter showed a steady Ag ion delivery avoiding an initial burst release that is sufficient to kill bacteria within several hours—clearly related to the release kinetics. Noticeable bacterial reduction was observed after about 4–6 h corresponding to a cumulative Ag release of $\sim 0.2 \mu\text{g cm}^{-2}$, yielding a minimum required Ag^+ concentration of $\sim 1.75 \mu\text{g ml}^{-1}$ (or $\sim 1.75 \text{ ppm}$) for *S. aureus* for the used conditions (here: 0.4 ml bacterial suspension

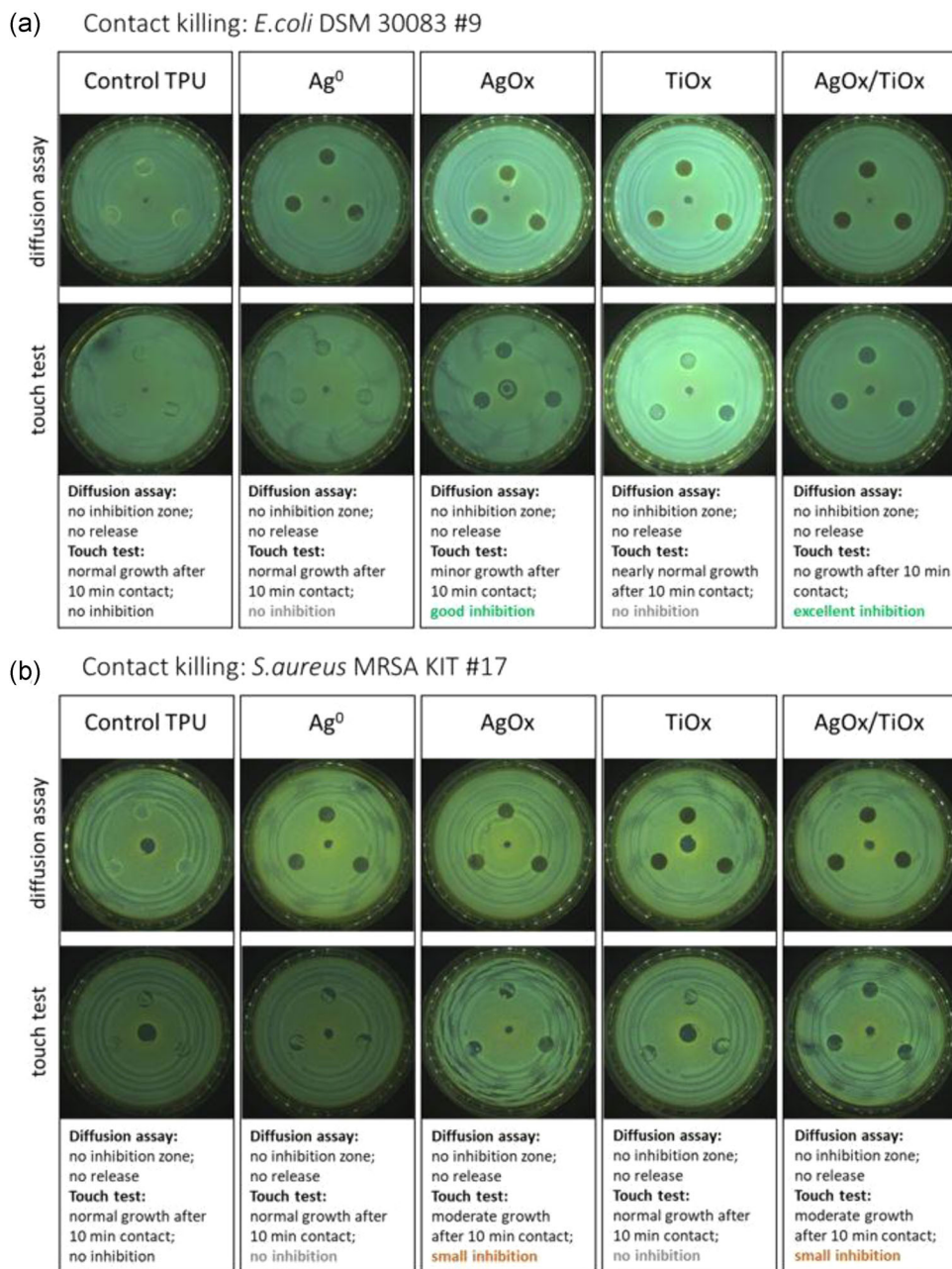


FIGURE 5 Diffusion assay (upper row) and touch test (lower row) for samples stored for 2 weeks in the dark tested against (a) *Escherichia coli* strain and (b) *Staphylococcus aureus* strain. While no sample revealed an inhibition zone by release effects during overnight incubation, only the oxidized Ag and the AgOx/TiOx catalyst showed antibacterial efficacy. TPU, thermoplastic polyurethane

on 3.5 cm² sample size), agreeing with findings for different Ag-containing coatings.^[4,5] After 10 days, about half of the deposited Ag content has been leached, slowly approaching saturation.

On the contrary, rapid-acting, minimally leaching antibacterial properties were obtained for the AgOx/TiOx coating, clearly corresponding to the ROS generation (Figure 9b). For example, after 1 h, Ag release of ~0.012 μg cm⁻² was noted for freshly prepared samples, yielding a concentration of ~0.075 ppm (0.1 ml bacterial

suspension on 0.64 cm² sample size), while *E. coli* bacteria already showed >5 log reduction. According to the literature, *E. coli* bacteria (MG 1655) also require Ag⁺ concentrations of around 1 ppm for a noticeable log-scale inhibition over a timescale of 6 h, probably slightly less than for *S. aureus*.^[57] Similar minimum bactericidal concentrations were reported for *E. coli* (DSMZ 6897) and *S. aureus* (DSMZ 1104) of 0.5–1.25 ppm and 1.25–2.5 ppm, respectively,^[58] leaving merely a small therapeutic window for Ag-releasing systems.^[59] After

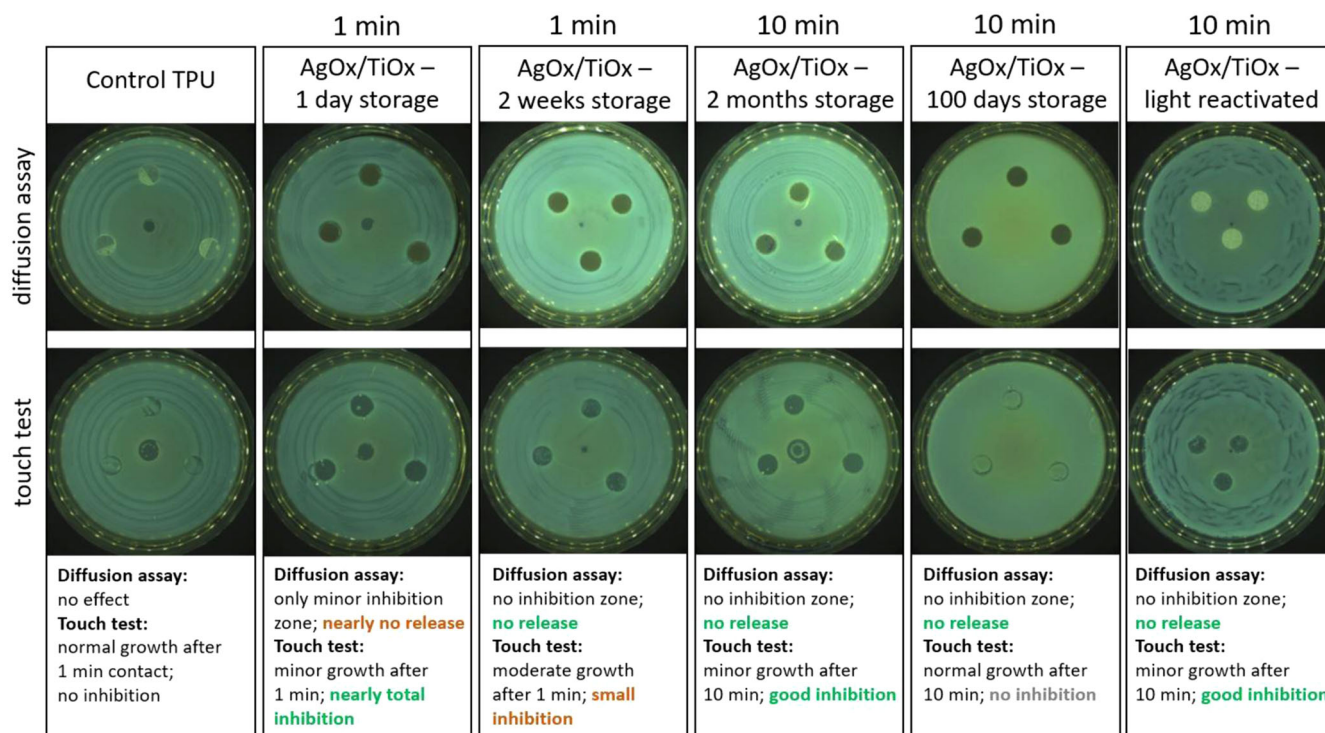


FIGURE 6 Diffusion assay (upper row) and touch test (lower row) for AgOx/TiOx samples stored for different periods in the dark. Initially, rapid contact killing appeared within 1 min (left). The antibacterial effect is attenuated with storage time but can be reactivated in visible light (far right). TPU, thermoplastic polyurethane

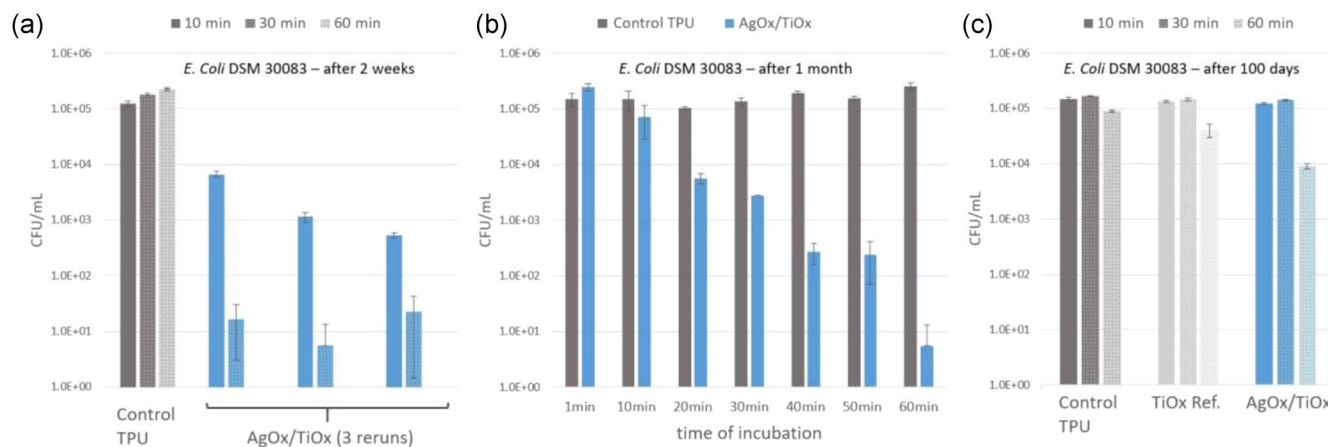


FIGURE 7 Modified ASTM method using *E. coli* strains to examine the antibacterial efficacy in solution (CFU, colony forming units). (a) Samples stored for 2 weeks in the dark, (b) after 1 month of storage, and (c) after 100 days in the dark. ASTM, American Society for Testing and Materials; TPU, thermoplastic polyurethane

6 h, a release of $\sim 0.068 \mu\text{g cm}^{-2}$ (~ 0.44 ppm) was measured for freshly prepared samples of AgOx/TiOx, which might account for the observed minor inhibition zone after overnight incubation in the diffusion assay. Moreover, the initial minor Ag ion release slowed down after several days of immersion in water, indicating stabilization of the coatings, well agreeing with the findings as discussed before. Note that the overall cumulative Ag

release content over 10 days from AgOx/TiOx corresponds to an average Ag thickness of ~ 0.2 nm, that is, less than one monolayer. Similar minimal releasing properties far below cytotoxicity levels have been reported for Ag₂O/ZrNO catalysts.^[60]

Accordingly, no cytotoxicity was noted for AgOx/TiOx samples (Figure 9c). Likewise, strongly H₂O₂-producing TiOx nanoparticles were reported to be generally safe and

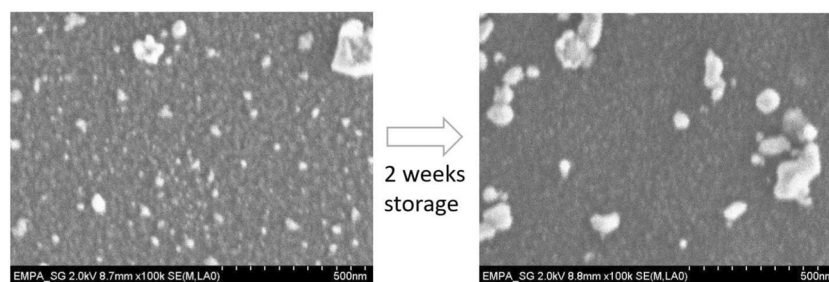


FIGURE 8 Scanning electron microscopy image of a freshly prepared AgOx-doped TiOx sample (left), which was stored for 2 weeks at ambient air in the dark (right). Tiny silver islands that can be observed within areas having less pronounced nanostructures disappear upon storage time

nontoxic, that is, causing no damage to liver, kidney, lung, or heart tissue.^[52] Ag⁰-containing films, on the contrary, induce Ag ion release-related cytotoxicity.^[5]

3.5 | Proposed mechanism

To enable further insights into the mechanism of the antibacterial activity of AgOx/TiOx catalysts, which was found to be preserved for a rather long period when stored in the dark and, most importantly, can be restored when exposed to visible light, samples stored in water and in ambient air (in the dark) were analyzed by SEM (Figure 10).

Ag⁰ formed larger particles upon storage in water, presumably by Oswald ripening with the strong release of Ag ions from the smaller particles until mainly the larger particles are left in agreement with the Ag ion release kinetics. It has been reported that oxidation of thin Ag films can largely suppress Oswald ripening, which should result in enhanced stability.^[61] Different from Ag⁰, for oxidized Ag, both storage in water and ambient air yielded growth to larger nano islands, maintaining the Ag island shape and Ag amount, probably related to Ag₂O reduction and self-stabilization.^[54] The change in morphology of the AgOx/TiOx catalyst was again different. Samples analyzed 1 day after deposition revealed pronounced Ag nano islets that developed into more particulate structures during extended storage times. XPS analyses revealed that the oxidized silver tends to be reduced to more metallic Ag during storage in the dark, as indicated by a positive shift toward the binding energies as observed for nonoxidized silver islands (Figure 11a). It can thus be assumed that this reduction process drove the observed restructuring. Interestingly, the changes in surface morphology were triggered by humidity when stored at ambient air in the same way as for storage in water, only following a different timescale. Similar findings on restructuring

processes upon storage in water or ambient air involving H₂O have been observed for various plasma-deposited metastable coating systems.^[60,62–64] Upon reduction of AgOx, the TiOx support became highly oxidized with few Ti³⁺ sites left after 1 year of storage in the dark (Figure 11b).

From the results obtained in this study, as well as from state-of-the-art, we can now propose a mechanism for the observed catalytic activity of AgOx-doped TiOx coatings when stored in the dark. We assume that dissolved O₂ can adsorb on the defective Ti³⁺/oxygen vacancy sites producing [•]O₂[−] by electron transfer, which is promoted by a synergetic effect between the O vacancy and the doped AgOx similar to the spontaneous CO₂ dissociation on defective Cu/Ti catalysts.^[27] Hence, ROS can be generated at the plasma-deposited catalyst surface even in the dark (Figure 12).

The proposed mechanism induces reduction of Ag₂O and filling of the O vacancy, resulting in the attenuation of ROS generation when stored in the dark, for example, in opaque packaging. However, the Ag nano islets supported on TiOx can be reactivated by visible light due to the excitation and reverse electron flow from the silver deposits to the CB of TiOx, resulting in reoxidation to Ag₂O within hours.^[37] Low-light conditions are thus sufficient to have a continuing ROS generating mechanism, which is used here for rapid antibacterial activity outperforming Ag releasing systems. Furthermore, the presented coatings comprising Ag nano islets on titanium suboxide might also be of interest for the photoreduction of cationic species and photo-oxidation of organics to treat toxic pollutants.^[65]

3.6 | Plasma functionalization

While freshly prepared or light-activated AgOx/TiOx coatings provide a highly wettable surface, storage in the dark retained a hydrophilic water contact angle of

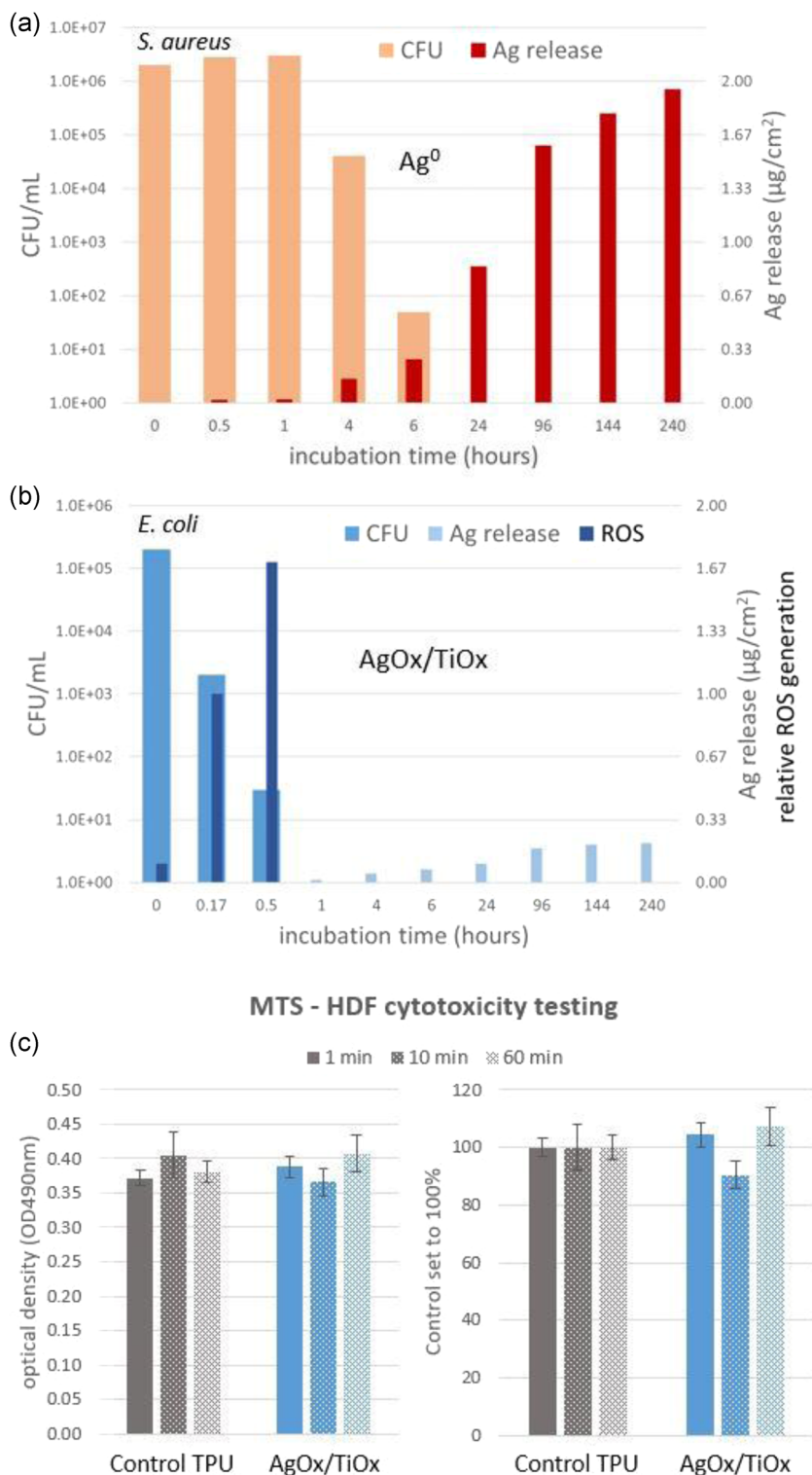


FIGURE 9 Antibacterial activity and biocompatibility: (a) 4 nm Ag^0 coating showing bacterial inhibition of *Staphylococcus aureus* according to the observed Ag ion release kinetic during incubation in water; (b) AgOx -doped TiOx coating revealing minimal Ag ion release within the first week of immersion in water, which stabilized afterward (below detection limit), whereas the rapid-acting antibacterial activity against *Escherichia coli* corresponds to ROS generation; (c) the AgOx/TiOx coatings, stored for 2 weeks in the dark, were found to be noncytotoxic, maintaining around 100% viable cells. ROS, reactive oxygen species; TPU, thermoplastic polyurethane

$50^\circ \pm 4^\circ$ during the entire study period of 2 years, which might be attributed to the sustained mild ROS generating properties even in the dark. As surface wettability strongly affects the binding strength and the number of interacting macromolecules at the biointerface,^[66] additional surface functionalization to adjust wettability becomes highly attractive, provided that the antibacterial

ROS mechanism can be maintained. Therefore, as a proof of principle, the use of plasma polymerization to functionalize the AgOx -doped TiOx coating was investigated by deposition of an ultrathin, 4-nm-thick hydrophobic layer using an Ar/HMDSO plasma.^[67] Such polydimethylsiloxane (PDMS)-like plasma polymer films allow transmission of oxygen and water vapor.^[68,69]

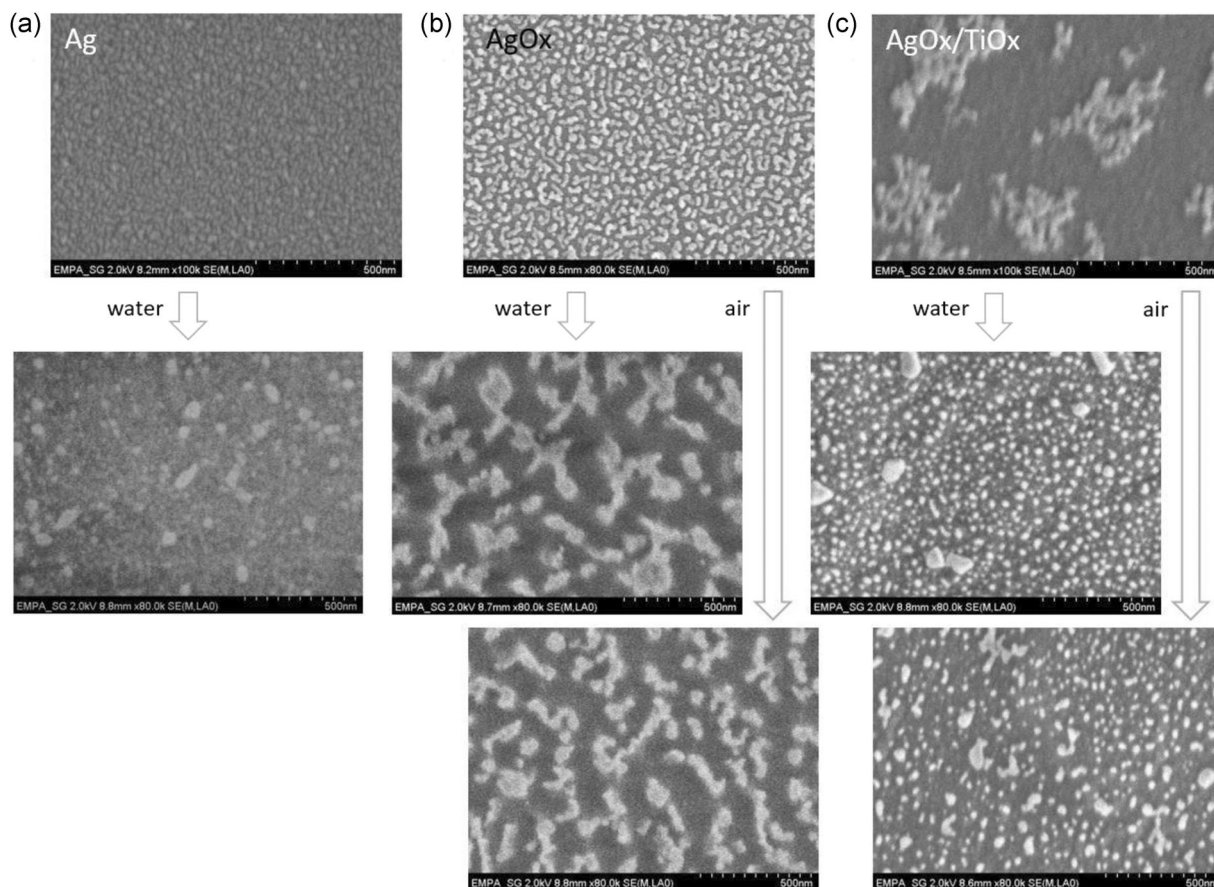


FIGURE 10 Samples were incubated for 2 weeks in water (in the dark) and 4 months stored at ambient air (in the dark). (a) Ag^0 forms some larger islands in the water, while most of the silver has been released. (b) Plasma oxidation results in more stable Ag structures independent of the storage in water or air. (c) Oxidized Ag dopant on the TiO_x support is reduced in the dark, showing comparable morphological changes when stored in water or air. The morphology becomes similar to Ag^0 stored in the water yet without noticeable Ag release

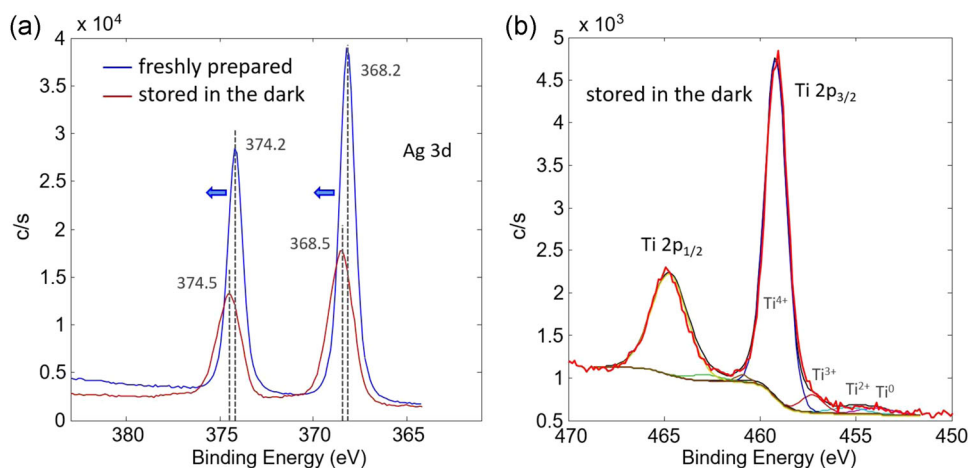


FIGURE 11 Long-term storage of AgOx/TiOx in the dark analyzed by X-ray photoelectron spectrometry: (a) AgOx is reduced to Ag^0 , (b) the TiO_x support is further oxidized mainly comprising TiO_2 in the near-surface region

To some extent, also water penetration occurs to a film depth of ~ 10 nm.^[33,70–72] Water might also find access to the catalyst surface through defects and phase boundaries in the hydrophobic cover layer caused by the

growth conditions on the Ag nano islet-decorated TiO_x surface (Figure 13a).

The presence of water and oxygen at the catalyst interface should thus promote the generation of ROS that

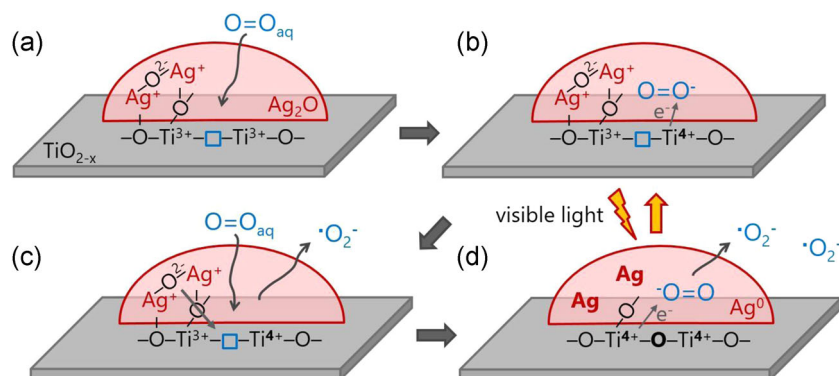


FIGURE 12 Schematic representation of the possible mechanism allowing ROS (reactive oxygen species) generation in the dark and reactivation by visible light at defective Ag/TiOx catalyst surfaces. (a, b) An electron is transferred to adsorbed O_2 at an oxygen vacancy (blue square), yielding the superoxide anion. (c, d) Further adsorbed O_2 can be reduced to $\cdot O_2^-$ without external activation, for example, in the dark; however, oxygen vacancies are filled, and Ag is reduced. (d)–(b) Visible light activation stimulates reoxidation of Ag, which restores the catalytic activity

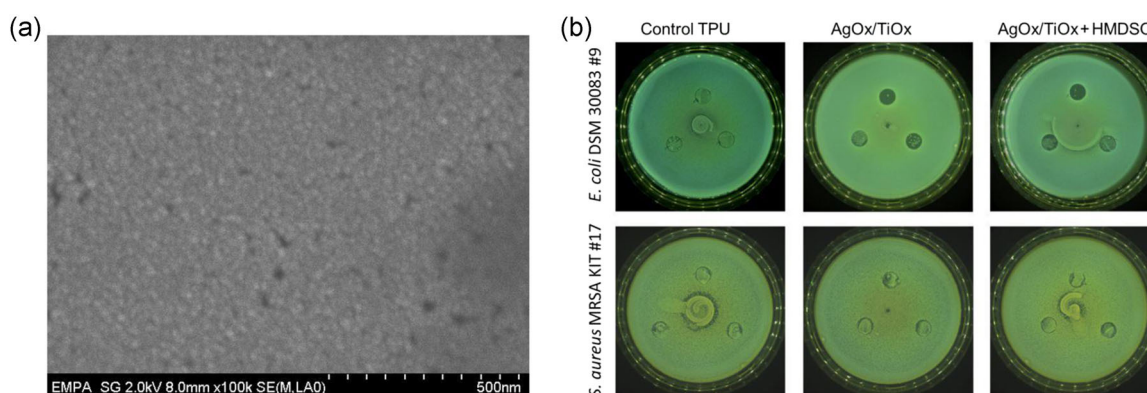


FIGURE 13 (a) Scanning electron microscopy image of a hexamethyldisiloxane (HMDSO)-coated Ag/TiOx catalyst surface indicating the formation of defects and phase boundaries within the 4-nm-thick plasma polymer layer. (b) Agar touch assay performed over 30 min with samples stored for 8 months in the dark, then light-activated for 10 h. Good inhibition was restored against *Escherichia coli* strains, also for HMDSO-functionalized AgOx/TiOx samples, while only minor inhibition was observed for *Staphylococcus aureus* strains. TPU, thermoplastic polyurethane

might diffuse out of the cover layer. Note that the surface functionalization should be resistant to the highly oxidizing conditions induced by $\cdot O_2^-$ and $\cdot OH$ production. Silicone coatings are generally able to resist such conditions and have thus been applied on various catalysts, including Ag/TiO₂, demonstrating that the catalytic activity can be maintained when water and oxygen can still reach the catalyst surface.^[73–75] Slight oxidation of deposited PDMS might even help to increase the photocatalytic activity of TiO₂ while stabilizing the catalyst.^[76] Compared to the reported wet-chemical coatings, plasma polymerization allows to adjust the thickness, crosslinking, nanoporosity, and wettability at the nanoscale.^[67]

To this end, AgOx/TiOx samples stored for 8 months in the dark were functionalized by the HMDSO-derived plasma layer yielding a water contact angle of $102^\circ \pm 3^\circ$

that was retained upon storage in ambient air followed over 6 months. The antibacterial efficacy was then assessed in an agar touch test after exposure to visible light for 10 h (Figure 13b). Both the reactivated AgOx/TiOx sample and the HMDSO-functionalized sample revealed good inhibition of *E. coli*. On the contrary, only a minor effect was observed for *S. aureus*, two out of three sample positions on the agar medium showed full overgrowth.

It has been reported that the Gram-positive *S. aureus* is mainly inactivated by singlet molecular oxygen.^[77] 1O_2 is a rather short-living radical with a half-life of $\sim 4 \mu s$ in water corresponding to a narrow diffusion length.^[51,78] It might thus be assumed that this radical is less effective for bacteria inactivation at the catalyst surface, especially for light-reactivated samples. More stable ROS such as hydrogen peroxide might thus indeed become the chief

antibacterial type as produced by quick conversion of $\cdot\text{O}_2^-$ to H_2O_2 .^[14] However, surface functionalization by plasma polymerization was found to be a suitable method.

4 | CONCLUSION

For many applications using materials in contact with biointerfaces that benefit from antibacterial surfaces, storage or use in the dark is a requirement: catheters, implants, percutaneous medical products, medical tubes and valves, wound dressings, air filtration, face masks, just to name a few. Furthermore, the potential release of toxic substances should be avoided allowing biocompatibility in all conditions. To fulfill such requirements, defective TiOx coatings were investigated as deposited by magnetron sputtering. Doping with Ag nano islands and subsequent plasma oxidation produced a catalyst surface showing a pronounced metal oxide nanostructure with a high interfacial area. Redox processes taking place at the catalyst surface when water and (dissolved) oxygen are present produce the highly oxidizing radicals, $\cdot\text{O}_2^-$ and $\cdot\text{OH}$, by electron transfer and oxidation at holes, respectively, promoted by oxygen vacancies in the plasma-deposited TiOx and narrow band gaps. Such radicals yield the generation of further ROS that have a strong antibacterial efficacy enabling contact killing within minutes directly at the catalyst surface but also efficient bacteria inhibition in a volume above the surface independent of the used solution. This ROS-generated antibacterial activity was significantly more rapid-acting than conventional Ag release systems, while only showing minor initial Ag ion release stabilizing upon storage. Most of all, storage at ambient air in the dark maintained antibacterial activity over at least 2 months; however, with decreasing efficacy due to attenuated production of ROS. Redox processes filling oxygen vacancies in TiOx accompanied by reduction of the Ag dopant are assumed to be responsible for the ongoing yet diminished activity in the dark. Importantly, the antibacterial activity can be restored by light stimulation using indoor lighting.

Furthermore, the AgOx/TiOx catalyst can be functionalized by deposition of a PDMS-like plasma polymer film providing a hydrophobic surface combined with ROS-mediated antibacterial properties. Such AgOx nano islet coatings on defective TiOx supports can be deposited in a one-step plasma process comprising plasma activation, Ti sputtering, Ag sputtering, and plasma post-oxidation—even applying an additional surface functionalization by plasma polymerization. Therefore, many industrial applications are opened up, where materials with sustained antibacterial properties are required to avoid not only the leaching of biocidal substances but also for various fields requiring catalytic surfaces.

ACKNOWLEDGMENT

We gratefully acknowledge financial support by Innosuisse—Swiss Innovation Agency (Project no. 30078.1 IP-LS). Open access funding provided by ETH-Bereich Forschungsanstalten. [Correction added on 13 May 2022, after first online publication: CSAL funding statement has been added.]

CONFLICT OF INTERESTS

The authors declare that there are no conflict of interests.

DATA AVAILABILITY STATEMENT

The data that support the findings of this study are available from the corresponding author upon reasonable request.

ORCID


Dirk Hegemann  <http://orcid.org/0000-0003-4226-9326>

Flavia Zuber  <http://orcid.org/0000-0003-1425-5920>

Fei Pan  <http://orcid.org/0000-0002-9801-5619>

Sandra Gaiser  <http://orcid.org/0000-0001-9111-2953>

Patrick Rupper  <http://orcid.org/0000-0001-5513-512X>

Katharina Maniura-Weber  <http://orcid.org/0000-0001-7895-3563>

Qun Ren  <http://orcid.org/0000-0003-0627-761X>

REFERENCES

- [1] P. W. Stone, *Expert Rev. Pharmacoecon. Outcomes Res.* **2009**, *9*, 417.
- [2] C. Adlhart, J. Verran, N. F. Azevedo, H. Olmez, M. M. Keinänen-Toivola, I. Gouveia, L. F. Melo, F. Crijs, *J. Hosp. Infect.* **2018**, *99*, 239.
- [3] L. Bonilla-Gameros, B. S. Chemistry, P. Chevallier, A. Sarkissian, D. Mantovani, *Nanomed. Nanotechnol. Biol. Med.* **2020**, *24*, 102142.
- [4] S. Lischer, E. Körner, D. J. Balazs, D. Shen, P. Wick, K. Grieder, D. Haas, M. Heuberger, D. Hegemann, *J. R. Soc., Interface* **2011**, *8*, 1019.
- [5] S. Wiesenmueller, P. Cierniak, M. Juebner, E. Koerner, D. Hegemann, K. Mercer-Chalmers *J. Biomater. Appl.* **2018**, *33*, 327.
- [6] C. Ma, A. Nikiforov, N. de Geyter, R. Morent, K. Ostrikov, *Curr. Opin. Chem. Eng.* **2022**, *36*, 100764.
- [7] L. Z. Flores-López, *J. Appl. Toxicol.* **2018**, *39*, 16.
- [8] S. A. Z. Estekhraji, S. Amiri, *J. Inorg. Organomet. Polym.* **2017**, *27*, 883.
- [9] M. Fiedot-Toboła, M. Ciesielska, I. Maliszewska, O. Rac-Rumijowska, P. Suchorska-Wozniak, H. Teterycz, M. Bryjak, *Materials* **2018**, *11*, 707.
- [10] J. Bogdan, J. Pławińska-Czarnak, J. Zarzyńska, *Nanoscale Res. Lett.* **2017**, *12*, 225.
- [11] Z. Zhou, B. Li, X. Liu, Z. Li, S. Zhu, Y. Liang, Z. Cui, S. Wu, *ACS Appl. Biol. Mater* **2021**, *4*, 3909.
- [12] A. U. Khan, M. Kasha, *Proc. Natl. Acad. Sci. U. S. A.* **1994**, *91*, 12365.
- [13] J. Kiwi, S. Rtimi, R. Sanjines, C. Pulgarin, *Int. J. Photoen.* **2014**, *2014*, 785037.

- [14] M. Y. Memar, R. Ghotaslou, M. Samiei, K. Adibkia, *Infect. Drug Resist.* **2018**, *11*, 567.
- [15] S. Rtimi, J. Kiwi, *Catalysts* **2021**, *11*, 201.
- [16] X. Pan, M. Q. Yang, X. Fu, N. Zhang, Y. J. Xu, *Nanoscale* **2013**, *5*, 3601.
- [17] M. D. Hernandez-Alonso, F. Fresno, S. Suarez, J. M. Coronado, *Energy Environ. Sci.* **2009**, *2*, 1231.
- [18] R. Daghrir, P. Drogui, D. Robert, *Ind. Eng. Chem. Res.* **2013**, *52*, 3581.
- [19] P. Lyu, J. Zhu, C. Han, L. Qiang, L. Zhang, B. Mei, J. He, X. Liu, Z. Bian, H. Li, *ACS Appl. Mater. Interfaces* **2021**, *13*, 2033.
- [20] M. Amberg, P. Rupper, R. Storchenegger, M. Weder, D. Hegemann, *Nanomed. Nanotechnol. Biol. Med.* **2015**, *11*, 845.
- [21] S. Rtimi, S. Giannakis, M. Bensimon, C. Pulgarin, R. Sanjines, J. Kiwi, *Appl. Catal., B* **2016**, *191*, 42.
- [22] S. A. Abdullah, M. Z. Sahdan, N. Nafarizal, H. Saim, Z. Embong, C. H. Cik Rohaida, F. Adriyanto, *Appl. Surf. Sci.* **2018**, *462*, 575.
- [23] I. Nakamura, N. Negishi, S. Kutsuna, T. Ihara, S. Sugihara, K. Takeuchi, *J. Mol. Catal. A: Chem.* **2000**, *161*, 205.
- [24] B. Bharti, S. Kumar, H. N. Lee, R. Kumar, *Sci. Rep.* **2016**, *6*, 32355.
- [25] H. Cao, Y. Qiao, X. Liu, T. Lu, T. Cui, F. Meng, P. K. Chu, *Acta Biomater.* **2013**, *9*, 5100.
- [26] S. Rtimi, S. Giannakis, R. Sanjines, C. Pulgarin, M. Bensimon, J. Kiwi, *Appl. Catal., B* **2016**, *182*, 277.
- [27] L. Liu, C. Zhao, Y. Li, *J. Phys. Chem., C* **2012**, *116*, 7904.
- [28] K. Nakata, A. Fujishima, *J. Photochem. Photobiol., C* **2012**, *13*, 169.
- [29] W. Nie, Q. Zhu, Y. Gao, Z. Wang, Y. Liu, X. Wang, R. Chen, F. Fan, C. Li, *Nano Lett.* **2021**, *21*, 8901.
- [30] R. E. Baier, A. E. Meyer, *Biofouling* **1992**, *6*, 165.
- [31] D. Hegemann, B. Hanselmann, N. Blanchard, M. Amberg, *Contrib. Plasma Phys.* **2014**, *54*, 162.
- [32] N. Subjaleeardee, D. Hegemann, M. Amberg, B. Hanselmann, P. Rupper, V. Intasanta, *Appl. Surf. Sci.* **2018**, *452*, 306.
- [33] N. E. Blanchard, B. Hanselmann, J. Drosten, M. Heuberger, D. Hegemann, *Plasma Processes Polym.* **2015**, *12*, 32.
- [34] D. Hegemann, N. Hocquard, M. Heuberger, *Sci. Rep.* **2017**, *7*, 17852.
- [35] E. Bülbül, P. Rupper, T. Geue, L. Bernard, M. Heuberger, D. Hegemann, *ACS Appl. Mater. Interfaces* **2019**, *11*, 42760.
- [36] M. Amberg, A. Haag, R. Storchenegger, P. Rupper, F. Lehmeier, R. M. Rossi, D. Hegemann, *Sci. Technol. Adv. Mater.* **2015**, *16*, 055002.
- [37] C. Gunawan, W. Y. Teoh, C. P. Marquis, J. Lifia, R. Amal, *Small* **2009**, *5*, 341.
- [38] P. Rupper, M. Amberg, D. Hegemann, M. Heuberger, *Appl. Surf. Sci.* **2020**, *509*, 145362.
- [39] R. Gouttebaron, D. Cornelissen, R. Snyders, J. P. Dauchot, M. Wautelet, M. Hecq, *Surf. Interface Anal.* **2000**, *30*, 527.
- [40] J. F. Moulder, W. F. Stickle, P. E. Sobol, K. D. Bomben, *Handbook of X-ray Photoelectron Spectroscopy*, Physical Electronics Inc, Eden Prairie, MN **1995**.
- [41] A. Gomes, E. Fernandes, J. L. F. C. Lima, *J. Biochem. Biophys. Methods* **2005**, *65*, 45.
- [42] A. Milonitis, A. Tripathy, M. Donati, C. S. Sharma, F. Pan, K. Maniura-Weber, Q. Ren, D. Poulidakos, *Ind. Eng. Chem. Res.* **2020**, *59*, 14323.
- [43] R. Nazir, D. Parida, J. Borgstädt, S. Lehner, M. Jovic, D. Rentsch, E. Bülbül, A. Huch, S. Altenried, Q. Ren, P. Rupper, S. Annaheim, S. Gaan, *Chem. Eng. J.* **2021**, *417*, 128028.
- [44] H. Volkmann, T. Schwartz, P. Bischoff, S. Kirchen, U. Obst, *J. Microbiol. Methods* **2004**, *56*, 277.
- [45] J. P. Meier-Kolthoff, R. L. Hahnke, J. Petersen, C. Scheuner, V. Michael, A. Fiebig, C. Rohde, M. Rohde, B. Fartmann, L. A. Goodwin, O. Chertkov, T. B. K. Reddy, A. Pati, N. N. Ivanova, V. Markowitz, N. C. Kyrpides, T. Woyke, M. Göker, H. P. Klenk, *Stand. Genom. Sci.* **2014**, *9*, 2.
- [46] F. Pan, S. Altenried, F. Zuber, R. S. Wagner, Y. H. Su, M. Rottmar, K. Maniura-Weber, Q. Ren, *Colloids. Surf., B* **2021**, *206*, 111940.
- [47] N. J. Firet, M. A. Blommaert, T. Burdyny, A. Venugopal, D. Bohra, A. Longo, W. A. Smith, *Mater. Chem. A* **2019**, *7*, 2597.
- [48] A. Zille, M. M. Fernandes, A. Francesko, T. Tzanov, M. Fernandes, F. R. Oliveira, L. Almeida, T. Amorim, N. Carneiro, M. F. Esteves, A. P. Souto, *ACS Appl. Mater. Interfaces* **2015**, *7*, 13731.
- [49] G. B. Hoflund, Z. F. Hazos, *Phys. Rev., B* **2000**, *62*, 11126.
- [50] S. Jana, A. K. Debnath, V. Putta, J. Bahadur, A. K. Chauhan, D. Bhattacharya, *Surf. Interface Anal.* **2021**, *53*, 509.
- [51] W. A. Pryor, *Ann. Rev. Physiol.* **1986**, *48*, 657.
- [52] M. Hassan, M. Nakayama, M. Salah, H. Akasaka, H. Kubota, M. Nakahana, T. Tagawa, K. Morita, A. Nakaoka, T. Ishihara, D. Miyawaki, K. Yoshida, Y. Nishimura, C. Ogino, R. Sasaki, *Nanomaterials* **2020**, *10*, 1125.
- [53] K. N. Pandiyaraj, D. Vasu, P. V. A. Padmanabhan, R. Ghobeira, P. S. E. Tabaei, P. Cools, N. de Geyter, R. Morent, R. R. Deshmukh, M. Pichumani, *Surf. Coat. Technol.* **2020**, *389*, 125642.
- [54] X. Wang, S. Li, H. Yu, J. Yu, S. Liu, *Chem.-Eur. J.* **2011**, *17*, 7777.
- [55] D. P. Kumar, N. L. Reddy, M. Karthik, B. Neppolian, J. Madhavan, M. V. Shankar, *Sol. Energy Mater. Sol. Cells* **2016**, *154*, 78.
- [56] C. N. Lok, C. M. Ho, R. Chen, Q. Y. He, W. Y. Yu, H. Sun, P. K. H. Tam, J. F. Chiu, C. M. Che, *J. Biol. Inorg. Chem.* **2007**, *12*, 527.
- [57] Y. M. Long, L. G. Hu, X. T. Yan, X. C. Zhao, Q. F. Zhou, Y. Cai, G. B. Jiang, *Int. J. Nanomed.* **2017**, *12*, 3193.
- [58] C. Greulich, D. Braun, A. Peetsch, J. Diendorf, B. Siebers, M. Epple, M. Köller, *RSC Adv.* **2012**, *2*, 6981.
- [59] S. L. Abram, K. M. Fromm, *Chem.-Eur. J.* **2020**, *26*, 10948.
- [60] S. Rtimi, M. Pascu, R. Sanjines, C. Pulgarin, M. Ben-Simon, A. Houas, J. C. Lavanchy, J. Kiwi, *Appl. Catal., B* **2013**, *138–139*, 113.
- [61] Y. Liu, C. F. Guo, S. Huang, T. Sun, Y. Wang, Z. Ren, *J. Materiomics* **2015**, *1*, 52.
- [62] M. Drábik, J. Pešička, H. Biederman, D. Hegemann, Long-term aging of Ag/a-C:H:O Nanocomposite coatings in air and in aqueous environment, *Sci. Technol. Adv. Mater.* **2015**, *16*, 025005.
- [63] P. Rupper, M. Vandenbossche, L. Bernard, D. Hegemann, M. Heuberger, *Langmuir* **2017**, *33*, 2340.

- [64] S. Kumar, J. Kratochvíl, Y. Al-Mukhrabi, O. Kylián, D. Nikitin, V. Straňák, *Plasma Processes Polym.* **2022**, *19*, e2100144.
- [65] K. Fujiwara, Y. Deligiannakis, C. G. Skoutelis, S. E. Pratsinis, *Appl. Catal., B* **2014**, *154–155*, 9.
- [66] E. Maikranz, C. Spengler, N. Thewes, A. Thewes, F. Nolle, P. Jung, M. Bischoff, L. Santen, K. Jacobs, *Nanoscale* **2020**, *12*, 19267.
- [67] D. Hegemann, E. Bülbül, B. Hanselmann, U. Schütz, M. Amberg, S. Gaiser, *Plasma Processes Polym.* **2021**, *18*, e2000176.
- [68] S. Steves, B. Ozkaya, C. N. Liu, O. Ozcan, N. Bibinov, G. Grundmeier, P. Awakowicz, *J. Phys. D: Appl. Phys.* **2013**, *46*, 084013.
- [69] M. Top, S. Schönfeld, J. Fahlteich, S. Bunk, T. Kühnel, S. Straach, J. T. de Hosson, *Surf. Coat. Technol.* **2017**, *314*, 155.
- [70] Y. Zhou, B. Josey, E. Anim-Danso, B. Maranville, J. Karapetrova, Z. Jiang, Q. Zhou, A. Dhinojwala, M. D. Foster, *Langmuir* **2018**, *34*, 9634.
- [71] E. Bülbül, D. Hegemann, K. Ataka, S. Lehner, J. Heberle, M. Heuberger, *Surf. Interfaces* **2021**, *23*, 100922.
- [72] D. Hegemann, S. Gaiser, *J. Phys. D: Appl. Phys.* **2022**, *55*, 173002.
- [73] J. Liu, L. Ye, S. Wooh, M. Kappl, W. Steffen, H. J. Butt, *Appl. Mater. Interfaces* **2019**, *11*, 27422.
- [74] S. Peng, W. Meng, J. X. Guo, B. Wang, Z. Wang, N. Xu, X. Li, J. Wang, J. Xu, *Langmuir* **2019**, *35*, 2760.
- [75] M. Ben Chobba, M. L. Weththimuni, M. Messaoud, C. Urzi, J. Bouaziz, F. de Leo, M. Licchelli, *Progr. Org. Coat.* **2021**, *158*, 106342.
- [76] M. G. Jeong, H. O. Seo, K. D. Kim, Y. D. Kim, D. C. Lim, *Thin Solid Films* **2012**, *520*, 4929.
- [77] H. Wu, P. Sun, H. Feng, H. Zhou, R. Wang, Y. Liang, J. Lu, W. Zhu, J. Zhang, J. Fang, *Plasma Processes Polym.* **2012**, *9*, 417.
- [78] A. Lavi, H. Weitman, R. T. Holmes, K. M. Smith, B. Ehrenberg, *Biophys. J.* **2002**, *82*, 2101.

How to cite this article: D. Hegemann, B. Hanselmann, F. Zuber, F. Pan, S. Gaiser, P. Rupper, K. Maniura-Weber, K. Ruffieux, Q. Ren, *Plasma Processes Polym.* **2022**;19:e2100246. <https://doi.org/10.1002/ppap.202100246>